JETIR.ORG ISSN: 2349-5162 | ESTD Year : 2014 | Monthly Issue
JOURNAL OF EMERGING TECHNOLOGIES AND INNOVATIVE RESEARCH (JETIR)
An International Scholarly Open Access, Peer-reviewed, Refereed Journal

Electro Paramagnetic Studies on as-synthesized Vanadium Sulphate impregnated Potassium Boro Dicitrate Single Crystal

Nagarajan Nithiya, Ravi Vinoth Kumar, Palanisamy Vickraman *

[1]Research Scholar, [2]Research Scholar, [3]Professor
[1]Solid State Ionics Lab, Department of Physics,
[1]The Gandhigram Rural institute – Seemed to be University, Gandhigram, India

Abstract : In the present study, single crystals of Potassium Boro di-citrate (KBDC-host) doped with vanadium sulphate (guest) at different concentrations from 0.1 g to 2 g are attempted by using slow evaporation technique. It is experimentally tailored that well defined single crystals only for four weight ratios namely 0.2, 0.5, 1, and 2 g of dopant are nucleated. From Electro Paramagnetic Resonance (EPR) studies, it is found that only 2.0 g doped KBDC showed higher absorption of EPR signal. Subsequently, the hyperfine splitting lines of this single crystal observed has been utilized to obtain g-tensor and A-tensor. These parameters have revealed that the crystal exhibits orthorhombic symmetry. Further, while comparing the bond length calculation of K-O and directional cosines associated with gzz tensor, VO2+ is found to be interstially placed within the host lattice. The Rache parameter (R) contented that the VO2+ is in d3z2-r2 ground state. Molecular orbital analysis of VO2+-KBDC indicating that the metal ligand bond showed characteristics of both ionic and covalent bonding. The Single Crystal X-ray Diffraction (XRD) unit cell crystalline parameters reveal the structural co-ordination of VO2+ and KBDC. The NLO study on this crystal indexing the second harmonic generation correspond to green light with 165 mV efficiency which is found to be 3 times higher than standard KDP single crystal. The photoluminescence studies on this crystal showed green light emission of 532 nm revealing the characteristics of vanadium.

Keywords - Pottasium boro dictrate; Electron Paramagnetic Resonance; Spin Hamiltonion Parameters; Second Harmonic Generation; Vanadium Sulphate.

Introduction

Electron paramagnetic resonance (EPR) spectroscopy is a versatile technique which explores intricacies of the crystalline symmetrical environment of the dopant how gets localized in selected host lattice. In other words, the localization symmetry of the guest species how gets coordinated in the crystalline boundaries can well be understood through canonical absorption of EPR signal with reference to the content of the concentration of guest rather sensitive to the EPR signal synagogue yield in synergistic effect on the benevolence grandeur of the host is subjected. [1,2]

A brevity among all transition metals, vanadium exhibits to exist in divalent, trivalent and tetravalent oxidation states wherein VO^{2+} observed to be exhibiting most stable. The appealing chemical and physical environment of vanadium ion embarking the crystalline environment of different host lattices contemplating the applications has been extensively browsed and studied. [3–5]

The scientific quests for comprehending non-linear optical (NLO) properties endowed with paramagnetic impurities doped single crystals implicitly invoked in the realm of materials science have indomitably contributing in the field of telecommunications and signal processing rather quivering optical modulation bestowed with optical data banking. In this line, the explicit emergence of envisioning such types of crystals showing their impeccable non-linear properties swiftly delved into the numerous investigations on organic – inorganic NLO crystals. [6–10] However, the perspectives of exploration on application have grounded profusely upon semi-organic single crystals (SOSCs) on account of progressive second harmonic signals (SHS). [11–13]

M.K.Dhatchayini et.al., investigated pure potassium borodicitrate (KBDC) semi-organic single crystal (borate family) and reported that it exhibited orthorhombic symmetry belonging to the space group of P_{bca}. The authors also attempted to study NLO properties by UV-Vis and confirmed KBDC crystal exhibits good transparency (80%) over the entire visible region and far IR region and noted that the cut-off wavelength occurred at 247 nm was due to the electronic transition from n orbital to π^* orbital.[14,15] Since physical properties such as photoconductivity, specific heat capacity and non-linear refractive index observations have paved the way for exploring EPR studies on this crystal with the paramagnetic ion as an impurity loaded into the crystal matrix has been attempted experimentally as well as theoretically to corroborate the imminence applications of such NLO crystals in many walks of life.[16,17] The efficiency of NLO crystals applications in optical gadgets have been found to dependent on donor-acceptor (D-p-A) configuration of the metal complexes rather acting as an electron acceptor predominantly bestowed with anions which improvise the efficiency of the NLO crystals.[18,19]

Thus to explore /comprehend /understand vividly the crystalline symmetry of KBDC how holds good to bias itself to invite paramagnetic impurity i.e. VO^{2+} how gets altering physical and chemical environment as a function of the variant of VO^{2+} weight ratio has been envisioned in the present work by EPR, SXRD, FTIR, EDAX, UV-VIS-NIR, SHG and Photoluminescence.

Methodology

The methodology is to identify the suitable compound of host as it chemically acts compatible through their mole ratio (stoichiometry) complexity in such a way that chosen tri-matrix as compound herein to be referred as host is appropriately selected based on the equation given below. [15]

$$KOH + H_3BO_3 + 2(C_6H_8O_7.H_2O) \rightarrow K[(C_6H_6O_7)_2.B].2H_2O \text{ -----(1)}$$

The second methodology is to vary VO^{2+} at four variants in constant KBDC (1:1:2) and study the EPR performance and other related physico-chemical parameters of both experimental and theoretical.

Synthesis of KBDC and mass dispersoid optimization of vanadium sulphate in-situ KBDC

In the present investigation, SOSCs are synthesized through controlled slow evaporation process in controlled atmosphere at ambient temperature, based on the stoichiometric of the chemical equation for the complexation (0.1mole of potassium hydroxide, 0.1 mole of boric acid and 0.2mole of di-citrate) to well defined semi-organic single crystal has been investigated as a pure KBDC. [15] The second complexing 0.1, 0.1, 0.2 mole ratio as a constant stoichiometry of KBDC infused with 0.1g to 2.0g in step difference of 0.1g of vanadium sulphate are attempted for nucleating unified single crystals. But the author could get SOSCs only for the four mass variant of vanadium sulphate (x= 0.2 g, 0.5g, 1.0g and 2.0 g). All these crystals so obtained are again subjected to recrystallization process furtherance for 15 days in order to have the better nucleated quality crystals so as to enhance the nonlinear characteristics by improvising the crystalline symmetry of the SOCSs crystals which are inadvertently evincing the quality of the single crystals both of pristine KBDC and VO^{2+} doped KBDC combinatorial four hybrid crystals alleviating the defects such as pores, cracks, clarity and adjoint nucleated morphic crystals are herein after labelled as KBDC@VS1(0.2g), KBDC@VS2(0.5g), KBDC@VS3(1g) and KBDC@VS4(2g). Amongst these four variates of vanadium sulphate, the 2.0 g vanadium sulphate infused in-situ to KBDC SOSC has shown a highly receptive response to the EPR signal in terms of its ability of absorption is very well noted in the present study. The detailed synthesizing route is given in the following illustration, Figure 1.

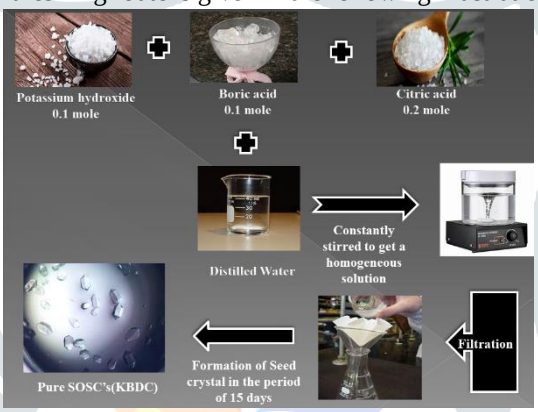

Figure 1a. The detailed synthesizing route of Pure KBDC

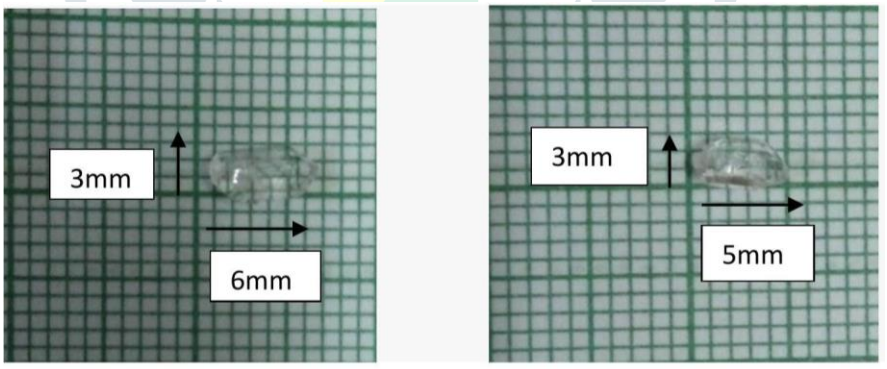

Figure 2. Image of KBDC-VO^{2+} and KBDC@VS4 single crystal

3. Results and Discussion

3.1 Single Crystal XRD studies

To comprehend the spatial symmetry of unit cell crystals which are characterizing the crystalline parameters which clearly reflecting the performance appraisal of as grown crystals as appended with the constituted lattice frame work revealing the coordination geometry of the host guest in interstially injection. The table 1 illustrates the unit cell parameters of pure and KBDC@VS4 are belonging to orthorhombic unit cell [16-18] and as tuned volume of the cells albeit a slight shift 6.9 Å3 (2.3 x 2.3 x 2.3) in it as found as obtained from XRD data may be caused by the VO2+ ion being interstially occupying into the crystal lattice framed by boron coordinated to hydroxyl and carboxyl functional group with end substituent hook-up VO2+ ions hangover found. [14,15]

Table 1. Comparison of Unit Cell Parameters

Lattice Parameters	Single crystal XRD	
	Pure KBDC	KBDC@VS4
a (Å)	10.110	10.115
b (Å)	11.170	11.180
c (Å)	33.135	33.120
α	90^0	90^0
β	90^0	90^0
γ	90^0	90^0
Volume($Å^3$)	3738.5	3745.4
Crystal system	orthorhombic	orthorhombic
Space group	P_{bca}	P_{bca}

3.2 Identification of Suitable SOSC by EPR Studies

Using the Bruker EMX plus spectrometer, EPR recording has been done by subjecting all single crystalsKBDC@VS1(0.2g), KBDC@VS2(0.5g), KBDC@VS3(1g) and KBDC@VS4(2g), in all three horizontal(H), vertical(V) and normal planes in 0°-180º angles @ 10° steps in each plane by rotating the quartz rod (wherein the single crystal is mounted) at 9.8 GHz X-band microwave frequency for magnetic modulation of 100 kHz.

Amongst the spectral observations onto all these single crystals, it is observed that 2g VO2+ doped KBDC has absorbed EPR signals more profoundly in all three mutually perpendicular H, V, and N planes resulting in eight well-defined distinct hyperfine lines referred as site A; and messy hyperfine lines within the site A are referred as site B, not taken for analysis due to poor response to EPR signal in all planes] as shown in Figure 3. The origin of this octant spectrum lies in the interplay between electron spin and the nucleus. [20,21] Thus the present investigation which identifies the 2g doped vanadium sulphate into the orthorhombic crystalline symmetry of KBDC crystal is proven to be for further studies (both theoretical and experimental EPR analysis) are discussed herein under to understand the metal-ligand complex endowed semi-organic crystal. [22]

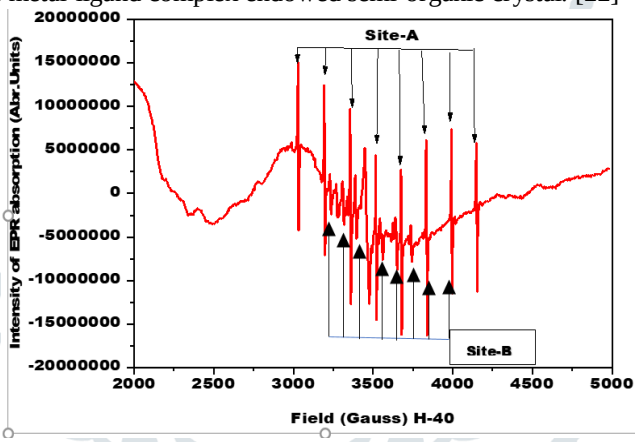

Figure 3. EPR spectrum for VO2+ doped KBDC single crystal along H-Plane at an angle of 40°rotations at room temperature.

3.3 Experimental and Theoretical Analysis of KBDC@VS4 SOSCs

3.3.1Angular Variations of KBDC@VS4

The external magnetic field (Hexp) values are measured from the site A in respective orthogonal planes: ab, bc, and ca, and their theoretical values are calculated by using the following Equation (2) (Htheor).

$$H_{theor} = H_{exp} - K_{m1} \text{ ----------(2)}$$

where H_{exp} experimental magnetic field, K- average experimental magnetic field, m_1 - Nuclear Zeeman splitting factor.

The experimental and theoretical values comprehend the angular variations of KBDC@VS4 in H-plane, V-plane and N-plane as illustrated in Figure 4 as a solid line and solid circle respectively. Both these observed and derived parameters of H values matching reveal the orthorhombic local symmetry of KBDCs, which is found to agree with the Jorgensen crystal field theory. [23]

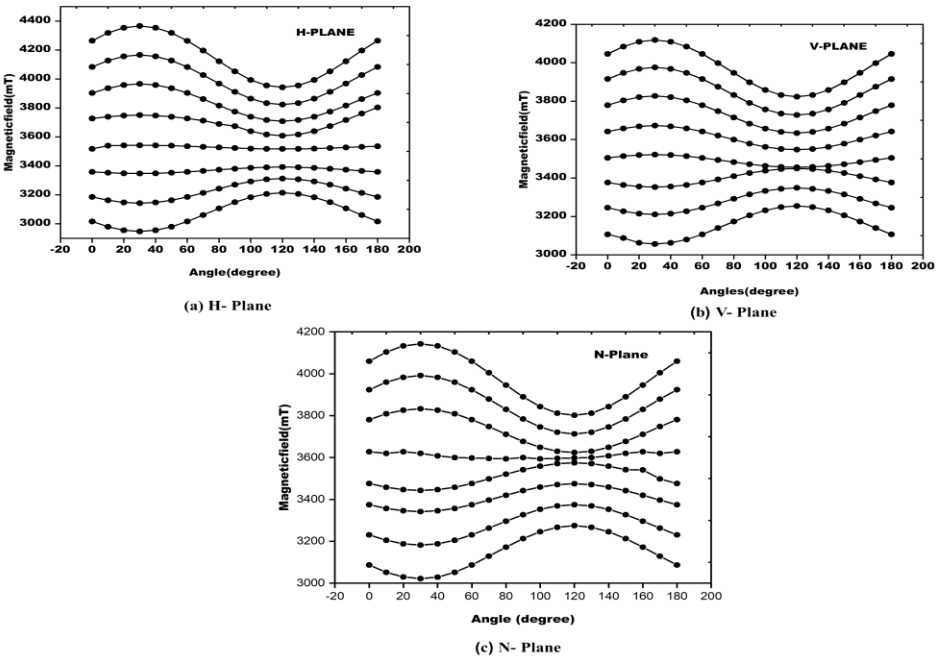

Figure 4: Angular difference spectra of VO2+doped KBDC of site-A.

3.3.2 Spin Hamiltonian Parameters (H) of KBDC@VS4

The spin Hamiltonian parameters (**H**) are calculated using the following equations.

$$H = \beta S.g.H + A.S.I \quad \text{----------(3)}$$

Where β - Bohr magneton, S -electron spin vector ($S=\frac{1}{2}$), I -Nuclear spin vector ($I=\frac{7}{2}$)m, g -spectroscopic splitting factor, H -applied magnetic field, A -Hyperfine splitting factor.

The g_{exp}, H_{exp} and A_{exp} are related by the following equations (4-4a, 4b) and equation (5) which are used to obtain experimental spin Hamiltonian parameters.

$$g_{exp} = \frac{h\upsilon}{\beta H_n} \quad \text{----------(4)}$$

$$(g_{exp})_{up} = \frac{h\upsilon}{\beta H_n(\theta_{up})} \quad \text{----------(4a)}$$

$$(g_{exp})_{low} = \frac{h\upsilon}{\beta H_n(\theta_{low})} \quad \text{----------(4b)}$$

$$A_{exp} = \frac{(H_n - H_1)}{n-1} \quad \text{----------(5)}$$

The theoretical spin Hamiltonian parameters are obtained using g_{theor}, A_{theor} at constant magnetic field as given in the equation (6).

$$g^2_{theory}(\theta) = \alpha + \beta\cos 2\theta + \gamma \sin 2\theta \quad \text{----------(6)}$$

where $\alpha = \left[\frac{\left(g^2_{exp.up} + g^2_{exp.low}\right)}{2}\right]$

$$\beta = \left[\frac{(g^2_{exp.up} - g^2_{exp.low})\cos 2\theta_{exp.up}}{2}\right]$$

$$\gamma = \left[\frac{(g^2_{exp.up} - g^2_{exp.low})\sin 2\theta_{exp.up}}{2}\right]$$

The upper and lower values of the g tensor, denoted as g_{up} and g_{low}, respectively. The angle θ represents the rotation of the crystal ranging from 0° to 180° across all three orthogonal planes H, V, and N at which $g_{ex.up}$ observed is denoted as $\theta_{exp.up}$. Equation (7) allows for the calculation of A_{theor}.

$$g^2_k(\theta)A^2_k(\theta) = g^2_{ii}A^2_{ii}cos^2\theta_i + g^2_{jj}A^2_{jj}cos^2\theta_j + 2g^2_{ij}A^2_{ij}sin\theta_i cos^2\theta_i \quad \text{--------(7)}$$

The coefficients g_{ii}, g_{jj}, g_{kk}, A_{ii}, A_{jj}, and A_{kk} are employed to determine the $g^2_k(\theta)A^2_k(\theta)$ values in 3 x 3 matrix tensors. These tensors are utilized to derive the direction cosines associated with the g tensor and A tensor of the spin Hamiltonian parameters (**H**).[24–26]

Table 2. Evaluation of spin Hamiltonian parameters (H) for KBDC@VS4

Site	g- Spectroscopic splitting tensor				A-Hyperfine splitting tensor			
		m	n	l		m	n	l
A	g_{xx}= 1.9246	0.1256	-0.9915	-0.0309	A_{xx}= 121	0.1999	0.9403	0.2753
A	g_{yy}=1.9857	0.6793	0.1087	-0.7256	A_{yy}=118	0.7483	-0.0347	0.6623
A	g_{zz}=1.9441	0.7229	0.0701	0.6873	A_{zz}=215	-0.6324	-0.3385	0.6967

3.3.3 Site Location Symmetry

The site location symmetry surrounding the VO2+ ion in the host crystal lattice is determined using the observed g_{xx}, g_{yy}, and g_{zz} values. [23] These g tensor values classify the three levels of symmetry based on the strength of the crystalline electric field and their corresponding orientations relative to the axes of the crystal field. If the g tensor satisfies the condition where $g_{xx} \neq g_{yy} \neq g_{zz}$, then it indicates that the impurity ion experiences a Weak crystal field, corresponding to orthorhombic symmetry, if the condition is $g_{xx} \neq g_{yy} = g_{zz}$, then it suggests that the impurity ion undergoes a Moderate crystal field, corresponding to axial symmetry, if g takes the form $g_{xx} = g_{yy} = g_{zz}$, then it signifies that the impurity ion is subjected to a Strong crystal field, corresponding to cubic symmetry. In the current investigation, the KBDC@VS4 complex satisfies the $g_{xx} \neq g_{yy} \neq g_{zz}$ (Table 2), indicating that the g tensor value at site-A reveals orthorhombic symmetry for the VO^{2+} ions in the host lattice with ligands. [24–26]

3.3.4 Position of the Impurity-ion

The crystallographic data is utilized for determining the location of the impurity site, Table 3 provides the direction cosines of the largest atom (K) bonding with various oxygen and water molecules in the KBDC system. These values serve as supporting evidence to verify the position of the paramagnetic impurity. [14] In the KBDC crystal, the bond length K-Ox (x = 1, 2, 3, 4, 9, 11) is generally associated with the principal gzz tensor values. The comparison of values from Table 2 and 3 reveals that the orientation of the gzz tensor does not align well with any of the bond directions in the KBDC crystal system. This observation suggests that the VO2+ ion tends to occupy an interstitial position rather than a substitutional site. Typically, if the atomic radii of the host ion (K) are larger, then which are replaced by the paramagnetic ion (VO2+) in a substitutional manner. However, in the current study, the presence of two chelate rings as part of the α-hydroxyl and carboxyl groups of two citrate ions results in a strong coordination between the boron atom and oxygen atom. As a result, the added impurity has infiltrated the lattice in an interstitial location. [27]

Table 3. The direction cosines of potassium with its surrounding atoms in the KBDC system

Bond	Bond length (A)	Direction cosines(orientation)		
		l	m	n
K–O_1	2.985	-0.3832	0.3596	0.3212
K–O_2	2.638	0.2389	0.5089	0.3156
K–O_3	3.141	-0.0856	0.2538	0.3450
K–O_4	3.157	0.0359	0.4288	0.3495
K–O_9	2.625	-0.1998	0.1548	0.4334
K–O_{11}	3.028	-0.1236	0.3943	0.4010
K–H_2O II	2.846	0.3788	0.2359	0.3834

3.3.5 Computing the Ground State Wave Function

In order to determine the energy level (ground state wave function) of the interstitial location, of the VO^{2+} ion within the host lattice, the Rache parameter (R) is utilized according to equation (8).

$$R = \frac{g_{yy}-g_{xx}}{g_{zz}-g_{yy}} \text{----------(8)}$$

If the value of R is less than one, the state exhibits a predominance of unpaired electrons, while if the value of R is greater than one, the state manifests an unpaired electron. Consequently, the ratio of the spectroscopic splitting factor in the present study, R is found to be 1.4687, which is greater than unity indicates that the VO2+ ion is in its ground state of $d_{3z^2-r^2}$.[20]

3.3.6 Computing Molecular Orbital Bonding Co-efficient

Molecular orbital analysis in EPR serves as a theoretical framework for comprehending the electronic structure and magnetic characteristics of paramagnetic species. It facilitates the interpretation of experimental data, prediction of spectroscopic features, and acquisition of insights into the chemical and physical factors that impact the magnetic properties of these systems.

The evaluation of the impurity ion's molecular orbital analysis is performed using the provided relations, and the results are presented in Table 4. The parallel and perpendicular components of the g and A tensor, denoted as (g⊥, g||, A⊥, and A||), are calculated based on the following relation.

$$g_{\perp} = \frac{g_{xx}+g_{yy}}{2} \;\&\; g_{\parallel} = g_{zz} \qquad (9)$$

$$A_{\perp} = \frac{A_{xx}+A_{yy}}{2} \;\&\; A_{\parallel} = A_{zz} \qquad (10)$$

It has been observed that the properties of the as-synthesized crystal exhibit variations depending on different crystallographic orientations, making it anisotropic. The determination of the parameter (g_{iso} and A_{iso}) is carried out using the following expressions (11) and (12).

$$g_{iso} = \frac{2g_{\perp}+g_{\parallel}}{3} \qquad (11)$$

$$A_{iso} = \frac{2A_{\perp}+A_{\parallel}}{3} \qquad (12)$$

The degree of d-electron delocalization, the unpaired spin density and the covalence nature of VO2+ are determined using the following equations and are presented in Table 4.

$$P = \frac{7(A_{\parallel} - A_{\perp})}{6} \quad (13)$$

$$k = -\frac{A_{iso}}{P} + (g_e - g_{iso}) \quad (14)$$

$$\alpha^2 = \frac{A_{\parallel}}{0.036} + g_{\parallel} - 2.0023 + \frac{3}{7}(g_{\perp} - 2.0023) + 0.04 \quad (15)$$

In the present study, the dipolar hyperfine coupling constant (P) is determined by calculating the ratio (Pcomplex / Pfree-ion) which corresponds to 31% for delocalization of the d-electron and 69% for the unpaired spin density of VO^{2+}, wherein the standard value of free ion is measured to be 360 $\times 10^{-4}$ cm^{-1}. The fermi contact term (k) is found to be 1.41, which is nearly equal to unity is related to the observed EPR signal which is directly proportional to the spin density of the unpaired electron and the bonding parameter (α2) 0.772, thereby elucidating the covalent nature of bonding between the metal and ion. [20]

Table 4. Molecular bonding coefficients of g and A of VO2+ ion in KBDC single Crystal at room temperature

Complex	$g_{\parallel}$	$g_{\perp}$	g_{iso}	$A_{\parallel}$	$A_{\perp}$	A_{iso}	P	k	α^2
KBDC-VO^{2+}	1.9551	1.9441	1.9514	215	119.5	151	111	1.41	0.77

3.4 FTIR Analysis

FTIR (Fourier Transform Infrared) analysis is based on the principle that different molecules absorb infrared light at specific frequencies called absorbance/ transmittance bands, provides valuable information about the molecular composition and structure of a substance. FTIR measurements are made for the as-synthesized single crystal utilizing a Perkin Elmer Spectrometer between the wavelength ranges of 4000 – 400 cm-1.

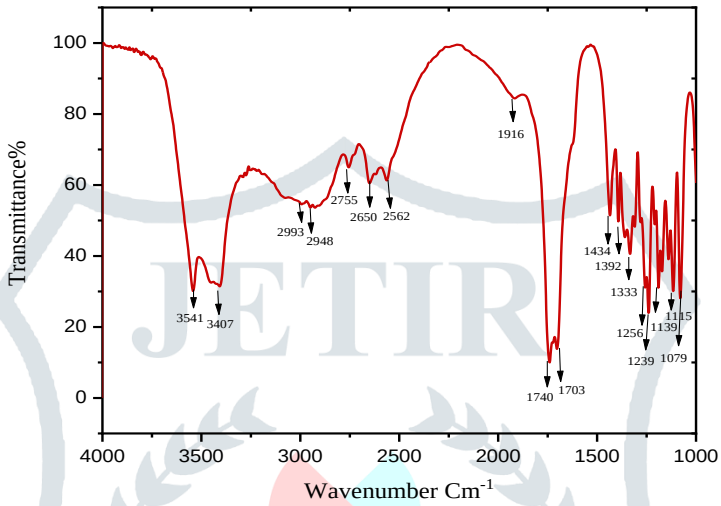

Figure 5a Functional group components of KBDC@VS4 in the higher wavenumber range between 1000 and 4000 cm^{-1}.

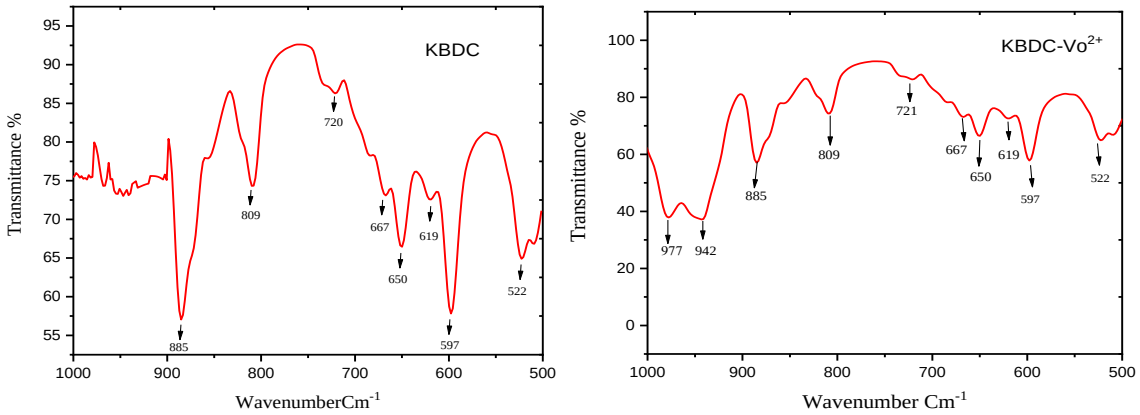

Figure 5. (b) FTIR spectra of KBDC and (c) Vo2+ doped KBDC single crystal in finger print zone between 500 and 800 cm^{-1}

In the case of KBDC, the existence of hydrate (H_2O) is confirmed by the O-H (sym. / asym.) stretching vibration at 3541 and 3407 cm^{-1}. The C-H stretching vibrations (sym. / asym.) are at 2993 and 2948 cm^{-1} [28,29]. Vibrational bands at1741 and 1702 cm^{-1} are assigned to C=O. The in-plane/ out-of-plane bending vibration associated with C-O has peaks at 1434, 1392, and 1359 cm^{-1}. The existence of the methylene group is confirmed by the peaks at 1333 and 1309 cm^{-1}. The transmittance band at 1115 cm^{-1} typically represents the presence of the C-O stretching vibration. The presence of the C-O-C stretching vibration is often indicated by the transmittance band at 1079 cm^{-1}. The B-O bending vibration is responsible for the peaks at 721 cm^{-1}. The C-H out-of-plane bending vibration is seen in the transmittance bands at 885 and 809 cm^{-1}. The O-H out of plane bending is shown by the peaks at 667, 650 and 619 cm^{-1}. Figure 5a depicts FTIR analysis for the presence of functional groups in pure and VO^{2+}-doped KBDC in the wave number range between 1000 and 4000 cm^{-1}. [30,31] The FTIR spectrum recorded after doping the paramagnetic impurity of VO^{2+} and its impact are compared to the pure KBDC spectrum. It is clearly evident that VO^{2+} is involved because a new absorbance band appears at 977 and 942 cm^{-1}, which matches (Table 5) to V-O in the fingerprint region between 400 and 1000 cm^{-1} in Figure 5 b and c. [32]

Table 5. FTIR values of KBDC@VS4 single crystal

Bands in cm^{-1}	Modes of vibrations
3541	O–H symmetric stretching
3407	O–H symmetric stretching
2993	C–H stretching
2948	C–H stretching
1740	C=O stretching
1703	C=C stretching
1434	Out of plane bending C–H
1392	Out of plane bending C–H
1359	Out of plane bending C–H
1115	C–O stretching
1079	C–O–C stretching
977	V–O asymmetric stretching
942	V–O symmetric stretching
885	Out of plane bending C–H
809	Out of plane bending C–H
721	Bending of B–O
667	Bending of B–O
650	Bending of B–O
619	Bending of B–O

3.5 EDAX Analysis

The EDAX mappings of pure KBDC and KBDC@VS4 single crystals are compared and noted that the presence of VO^{2+} in the later sample confirming the complex formation of vanadium with KBDC and its percentile is given in Table 6. [4,24]

Table 6. EDAX assessments of Pure KBDC and KBDC@VS4 single crystal

S. No.	Elements	Atomic%	
		Pure KBDC	KBDC-VO2+
1.	C	36.16	34.25
2.	O	44.18	42.38
3.	K	19.66	23.17
4.	V	----	0.20

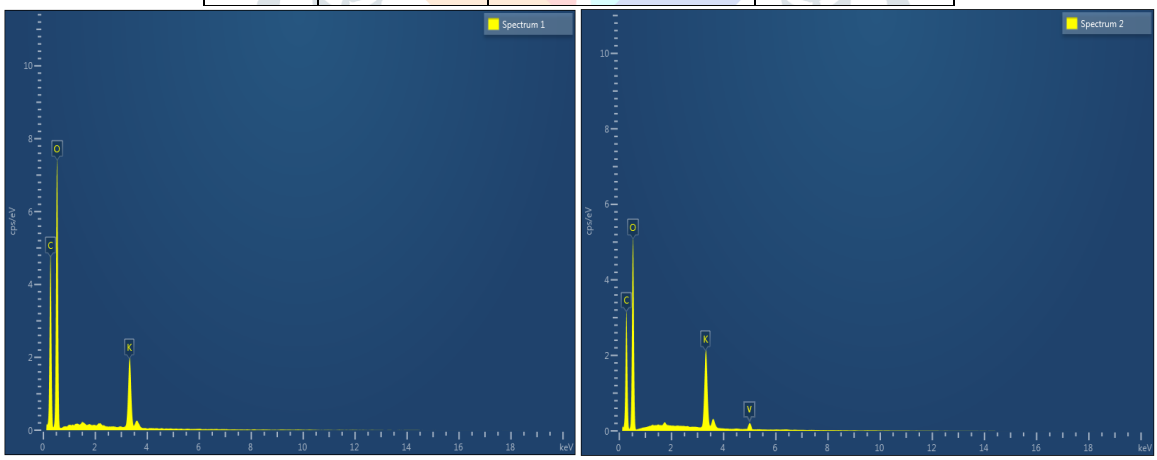

Figure 6. EDAX Spectrum of Pure KBDC and KBDC@VS4 single crystal

3.6 Optical Property Analysis

3.6.1 UV-VIS-NIR Spectral Analysis

The optical absorption spectrum of the KBDC@VS4 single crystal is measured using a Perkin Elmer Lambda-35 UV-VIS-NIR spectrometer at room temperature in the wavelength range 200 nm to 800 nm. Figure 7 shows three absorption bands for the VO^{2+} ion corresponding to d-d transitions, the first band located at 509nm, corresponds to $\Delta_{\perp} = {}^2B_{2g} \leftrightarrow {}^2E_{2g}\ (d_{xy} \leftrightarrow d_{xz,yz})$ transition, the second band at 600nm, is assigned to the $\Delta_{\parallel} = {}^2B_{2g} \leftrightarrow {}^2B_{1g}\ (d_{xy} \leftrightarrow d_{x^2-y^2})$)) transition and finally the third band at 710 nm, is associated with the $\Delta = {}^2B_{2g} \leftrightarrow {}^2A_{1g}\ (d_{xy} \leftrightarrow d_{z^2})$ transition.[33]

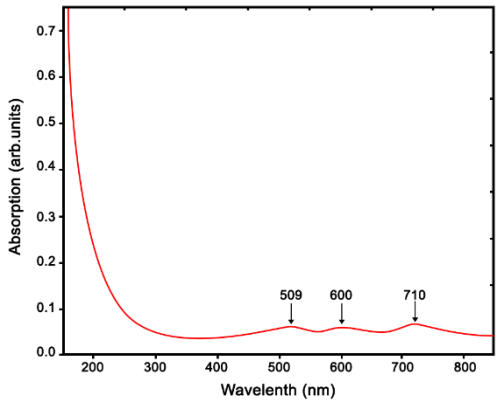

Figure 7. UV Spectrum of KBDC@VS4 single crystal

3.6.2 Non Linear Optical Studies

The Kurtz powder technique is widely employed for identifying materials with non-centrosymmetric crystal structures and confirming the second harmonic generation (SHG) efficiency of nonlinear optical (NLO) materials [30]. To verify the NLO behaviour of these materials, powdered samples were subjected to the Kurtz and Perry powder technique. A Q-switched Nd: YAG laser beam with a wavelength of 1064 nm, a pulse width of 10ns, and an input rate of 10Hz was used to test the NLO property of the sample. The KBDC@VS4 sample is prepared in powder form and filled into a micro capillary tube with a uniform bore of approximately 1.5 mm in diameter. The laser beam is directed perpendicularly onto the sample cell after passing through an infrared (IR) reflector. The microcrystalline powdered sample is served as the target for the incident laser beam. The second harmonic generation (SHG) radiation, which emitted green light at a wavelength of 530 nm, is collected using a photo multiplier tube (PMT) of Hamamatsu model R2059. The SHG output efficiency is compared with the KDP, a well-established inorganic material with nonlinear optical (NLO) properties. It is noted that SHG efficiency of KBDC@VS4 is 165mV whereas KDP is 55 mV which is found to be 3 times higher than KDP crystal might be implying towards using it as a UV filter and as a source in opto-electronic device. [33]

3.6.3 Photoluminescence (PL) spectral studies

The as-selected KBDC@VS4 single crystals is subjected to Photoluminescence studies. The photoluminescence spectrum is acquired at room temperature using an excitation wavelength of 243 nm shown in Figure 8 and within that a strong intense emission peak at 530 nm (equivalent to 5.1659 eV) is observed, indicative of the presence of near band-edge excitons within this crystal. Furthermore, the complete absence of discernible emission bands in the spectrum brings forth a clear evidence indicative of the good transparency of the crystal owing to its perfect crystallinity suggesting for its applications. [33]

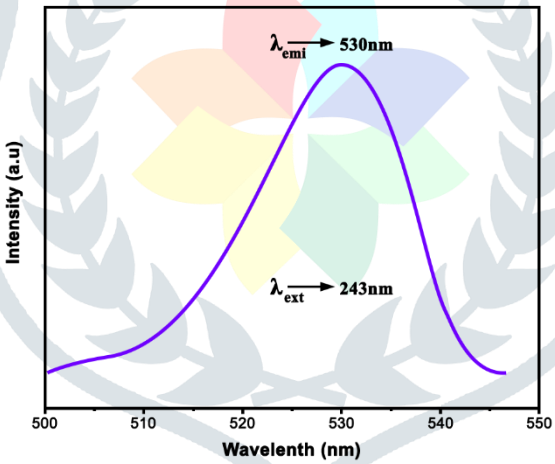

Figure 8. PL Spectrum of KBDC@VS4 single crystal

Conclusion

SXRD investigations into unit cell parameters indicate that both pristine KBDC and KBDC single crystals with dispersed VO^{2+} exhibit orthorhombic symmetry. The maximum absorption of the EPR signal was observed in 2g of VO^{2+} in KBDC. Angular variation calculations using spin Hamiltonian parameters, including spectroscopic splitting (g) tensor values and hyperfine splitting (A) tensor values, support the SXRD findings which are consistent with Jorgensen field theory on local field symmetry. The bond lengths K–O and direction cosines of g-tensor values confirm the interstitial placement of VO^{2+} ions. Molecular orbital analysis, as indicated by the Rache parameter, affirms the prevailing presence of VO^{2+} in a state that exhibits characteristics of both ionic and covalent bonding. FTIR studies confirm the complexation of VO^{2+} through its presence in the fingerprint region. EDAX confirms the presence of VO^{2+} in the impure KBDC crystal through the level of absorption. The optical absorption spectra reveal three absorption bands corresponding to distinct transitions: the d-d for KBDC@VS4 SOSC. The crystal exhibited a second harmonic generation efficiency is three times greater than that of the standard potassium dihydrogen phosphate crystal. The PL study shows the perfect crystalline nature of as-grown KBDC@VS4 crystal.

Reference

[1] S. Radhakrishna, M. Salagram, Orientational (EPR) study of vanadyl ion in potassium hydrogen oxalate lattice, Solid State Commun. 47 (1983) 77–82. https://doi.org/10.1016/0038-1098(83)90099-6.

[2] V.K. Jain, EPR of Mn2+ and VO2+ in K2C2O4 · H2O Single Crystals, Phys. Status Solidi. 97 (1980) 337–344. https://doi.org/10.1002/pssb.2220970139.

[3] R. Kripal, A. Mishra, Estimation of ground state wave function and nature of bonding of paramagnetic ion in vanadyl doped single crystals, Chem. Phys. Lett. 478 (2009) 307–309. https://doi.org/10.1016/j.cplett.2009.07.068.

[4] K. Juliet sheela, S. Radha Krishnan, V.M. Shanmugam, P. Subramanian, EPR and optical studies of VO2+ doped potassium succinate-succinic acid single crystal – Substitutional incorporation, J. Mol. Struct. 1131 (2017) 149–155. https://doi.org/10.1016/j.molstruc.2016.11.005.

[5] B. Karabulut, A. Tufan, An EPR and optical absorption study of VO2+ ions in sodium hydrogen oxalate monohydrate (NaHC2O4·H2O) single crystals, Spectrochim. Acta - Part A Mol. Biomol. Spectrosc. 65 (2006) 742–748. https://doi.org/10.1016/j.saa.2006.01.002.

[6] P.N. Prasad, D.J. Williams, INTRODUCTION TO MOLECULES AND EFFECTS IN NONLINEAR OPTICAL POLYMERS, John Wiley & Sons, Inc., 1991.

[7] V. Thendral, P. Suganthi, G. Marudhu, A. Thayumanavan, Growth, structural, vibrational, optical, mechanical studies of Boric acid doped KAP single crystal, Int. J. ChemTech Res. 11 (2018) 231–238. https://doi.org/10.20902/ijctr.2018.110326.

[8] K. Vasantha, P.A. Mary, S. Dhanuskodi, Epr and optical absorption studies of vo(ii)-doped zinc tris thiourea sulfate, Spectrochim. Acta - Part A Mol. Biomol. Spectrosc. 58 (2002) 311–316. https://doi.org/10.1016/S1386-1425(01)00535-2.

[9] S.G. Bhat, S.M. Dharmaprakash, Crystal growth and characterization of antimony thiourea bromide, J. Cryst. Growth. 181 (1997) 390–394. https://doi.org/10.1016/S0022-0248(97)00283-2.

[10] Y.M. Dai, J.K. Cheng, J. Zhang, E. Tang, Z.J. Li, Y.H. Wen, Y.G. Yao, Synthesis, structure, and fluorescence of two cadmium(II)-citrate coordination polymers with different coordination architectures, J. Mol. Struct. 740 (2005) 223–227. https://doi.org/10.1016/j.molstruc.2005.01.031.

[11] M. Yildirim, A.S. Kipcak, F.T. Senberber, M.O. Asensio, E.M. Derun, S. Piskin, The Determination of the Potassium Nitrate , Sodium Hydroxide and Boric Acid Molar Ratio in the Synthesis of Potassium Borates via Hydrothermal Method, 9 (2015) 605–608. scholar.waset.org/1307-6892/10001632.

[12] T. Sasaki, Y. Mori, M. Yoshimura, Y.K. Yap, T. Kamimura, Recent development of nonlinear optical borate crystals: Key materials for generation of visible and UV light, Mater. Sci. Eng. R Reports. 30 (2000) 1–54. https://doi.org/10.1016/S0927-796X(00)00025-5.

[13] C. Ramki, R.E. Vizhi, Synthesis and characterization of inorganic nonlinear optical material: Potassium sodium hydroxide borate hydrate (KSB) single crystal, Mater. Lett. 188 (2017) 156–158. https://doi.org/10.1016/j.matlet.2016.11.034.

[14] K.C.H.O.T. B, I.I. Zviedre, V.S. Fundamenskii, Crystal Structure of Pottasium Borodicitrate (Dicitratoborate), Plenum Publ. Corp. 25 (1985) 95–101.

[15] M.K. Dhatchaiyini, G. Rajasekar, A. Bhaskaran, Synthesis, growth, optical, photoconductivity and specific heat properties of potassium borodicitrate (KBDC) single crystal, J. Mater. Sci. (2019). https://doi.org/10.1007/s10853-019-03542-4.

[16] N. Nagarajan, V. Palanisamy, EPR Analysis of Cu2+ ion Doped Potassium borodicitrate Single Crystal, Trends Sci. 19 (2022). https://doi.org/10.48048/tis.2022.1917.

[17] V.K. Ravi, P. Vickraman, T.A. Raja, Investigation of Benzene 1,4-Dicarboxylic Acid MOF Linker Encapped Zinc Phosphate @ rGO-Based Binder-Free Electrode for Hybrid Supercapacitor Applications, Phys. Status Solidi Appl. Mater. Sci. 220 (2023) 1–14. https://doi.org/10.1002/pssa.202300210.

[18] Z. Yarbaşi, B. Karabulut, A. Karabulut, EPR and UV studies of VO2+ ions in potassium d-gluconate monohydrate single crystals, Phys. B Condens. Matter. 404 (2009) 3694–3697. https://doi.org/10.1016/j.physb.2009.06.116.

[19] P. Subramanian, K. Juliet sheela, S. Radha Krishnan, V.M. Shanmugam, Elucidation of site symmetry, location, bond, ground state of Cu2+ ions in lithium sulphate monohydrate single crystal through EPR and optical studies, J. Mol. Struct. 1206 (2020) 127586. https://doi.org/10.1016/j.molstruc.2019.127586.

[20] D.S. Schonland, On the determination of the principal g-values in electron spin resonance, Proc. Phys. Soc. 73 (1959) 788–792. https://doi.org/10.1088/0370-1328/73/5/311.

[21] B. Karabulut, F. Düzgün, An EPR study of Cu2+ doped [Na(Hmal)(H2O)5] single crystals, Spectrochim. Acta - Part A Mol. Biomol. Spectrosc. 75 (2010) 1200–1202. https://doi.org/10.1016/j.saa.2009.11.036.

[22] P. Dwivedi, R. Kripal, M.G. Misra, EPR and optical absorption studies of Cu2+ ions doped magnesium citrate decahydrate single crystals, J. Alloys Compd. 499 (2010) 17–22. https://doi.org/10.1016/j.jallcom.2010.03.126.

[23] E. Poonguzhali, R. Srinivasan, R. Venkatesan, R.V.S.S.N. Ravikumar, P. Sambasiva Rao, Variable temperature EPR study for confirming dynamic Jahn-Teller distortion in Cu(II) doped zinc ammonium phosphate hexahydrate, J. Phys. Chem. Solids. 64 (2003) 1139–1146. https://doi.org/10.1016/S0022-3697(03)00040-4.

[24] K. Juliet sheela, P. Subramanian, Influence of VO2+ ions on structural and optical properties of potassium succinate-succinic acid single crystal for non-linear optical applications, Phys. B Condens. Matter. 534 (2018) 156–162. https://doi.org/10.1016/j.physb.2018.01.028.

[25] D. Srinivas, M.V.B.L.N. Swamy, S. Subramanian, E.P.R. Of cu(II) in dinitratobis(antipyrine)zinc(II) single crystals: A case of low symmetry and mixed ground state, Mol. Phys. 57 (1986) 55–63. https://doi.org/10.1080/00268978600100041.

[26] U.B. Gangadharmath, S.M. Annigeri, A.D. Naik, V.K. Revankar, V.B. Mahale, Synthesis, characterisation and evaluation of molecular-orbital parameters, spin-orbit, dipolar and fermi-contact terms of VO2+ ion in thiosemicarbazone complexes, J. Mol. Struct. THEOCHEM. 572 (2001) 61–71. https://doi.org/10.1016/S0166-1280(01)00564-4.

[27] H.J. Prochaska, W.F. Schwindinger, M. Schwartz, M.J. Burk, E. Bernarducci, R.A. Lalancette, J.A. Potenza, H.J. Schugar, Characterization of Apical Copper(11)-Thioether Bonding. Structure and Electronic Spectra of Bis(2,2-bis(5-phenyl-2-imidazolyl)propane)copper(11) Diperchlorate and Bis(1,3-bis(5-phenyl-2-imidazolyl)-2-thiopropane)copper(11) Diperchlorate, J. Am. Chem. Soceity. (1981) 3446–3455.

[28] V.K. Ravi, V. Palanisamy, A.R. Thomai, M.S. Ramya Bharathi, 2D carbon nanofiber-augmented copper ammonium phosphate for hybrid supercapacitor device applications, J. Mater. Sci. Mater. Electron. 34 (2023) 2201–2216. https://doi.org/10.1007/s10854-023-11488-2.

[29] T.A. Raja, P. Vickraman, V.K. Ravi, Cucumis melo var agrestis based activated carbon / manganese ammonium phosphate @ carbon hollow sphere in dual redox additives for supercapattery device, Energy Storage. (2023) 1–18. https://doi.org/10.1002/est2.495.

[30] J. Coates, Interpretation of Infrared Spectra, A Practical Approach, Infrared Spectr. Interpret. A Syst. Approach. (2000) 10815–10837. https://doi.org/10.1201/9780203750841.

[31] Enrique J. Barana and Kwang-Hwa Lii, Vibrational Spectra of the Layered Compound [(VO2)2(4,4-bipy)0.5(4,4†-Hbipy)(PO4)]·H2O, Society. 2 (2005) 4583–4590.

[32] D. Peak, G.W. Luther, D.L. Sparks, ATR-FTIR spectroscopic studies of boric acid adsorption on hydrous ferric oxide, Geochim. Cosmochim. Acta. 67 (2003) 2551–2560. https://doi.org/10.1016/S0016-7037(03)00096-6.

[33] S. Sudhahar, M. Krishna Kumar, A. Silambarasan, R. Muralidharan, R. Mohan Kumar, Studies on Structural, Spectral, and Optical Properties of Organic Nonlinear Optical Single Crystal: 2-Amino-4,6-dimethylpyrimidinium p-Hydroxybenzoate, J. Mater. 2013 (2013) 1–7. https://doi.org/10.1155/2013/539312.